# Toward a new description of triaxial nuclei

A. A. Raduta[1,2] and P. Buganu[1]

[1]*Department of Theoretical Physics, Institute of Physics and Nuclear Engineering, Post Office Box MG6, RO-077125 Bucharest, Romania*

[2]*Academy of Romanian Scientists, 54 Splaiul Independentei, RO-050094 Bucharest, Romania*

(Received 5 January 2011; published 14 March 2011)

The liquid drop Hamiltonian is amended with a potential which allows us to separate, in the intrinsic frame, the equations for $\beta$ and $\gamma$ coordinates. The Schrödinger equation for $\beta$ is that for a sextic oscillator plus a centrifugal term, while that for $\gamma$ is just the equation for the Mathieu function. The total energy has a compact form. The operator for the electric quadrupole transitions is considered in the intrinsic frame and involves two parameters accompanying the harmonic and anharmonic components. The parameters determining the energies as well as those defining the transition operator are to be determined by a fitting procedure. Applications refer to five isotopes: $^{188}$Os, $^{190}$Os, $^{192}$Os, $^{228}$Th, and $^{230}$Th. Results are in good agreement with the corresponding experimental data. Results are also compared with those obtained within the coherent state model. A possible connection between the two formalisms is pointed out.

DOI: 10.1103/PhysRevC.83.034313 PACS number(s): 21.10.Re, 21.60.Ev, 27.70.+q

## I. INTRODUCTION

The first phenomenological approach [1] for nuclear energy levels and transition probabilities, known as the liquid drop model (LDM), has some natural limitations caused by the fact that it considers a harmonic drop. Many improvements have been proposed to describe oscillations around deformed equilibrium shapes [2] or to account for anharmonicities [3,4]. The drawback of the anharmonic model consists in the large number of parameters involved. Although it is hard to reduce the number of parameters and still provide a realistic description of the complex nuclei, some attempts have been made. Thus, the triaxial rigid rotor approach [5] and its improvements [6,7] consider a special class of nuclei without any symmetry axis. In [5], the $\beta$ and $\gamma$ have rigid values, the energies being determined by the motion of Euler angles specifying the intrinsic frame. The improvements refer to relaxing the rigidity and considering either a soft $\beta$ or a soft $\gamma$ variable. Exploiting the semiclassical features of the nuclear states of high angular momentum, the coherent state model (CSM) defines [8] the first three rotational bands by projecting out the angular momentum from a coherent state and two orthogonal polynomial excitations. The three sets of states are approximate eigenstates of a quadrupole boson Hamiltonian. The model is able to describe in a realistic fashion transitional and well-deformed nuclei of various shapes including states of high and very high angular momentum. Various extensions to include other degrees of freedom such as isospin [9], single-particle [10], or octupole [11,12] degrees of freedom have been formulated [13].

It has been noticed that a given nuclear phase may be associated with a certain symmetry. Hence, its properties may be described with the help of the irreducible representation of the respective symmetry group. Along this line, the interacting boson approximation (IBA) [14,15] succeeded in describing the basic properties of a large number of nuclei in terms of the symmetries associated with a system of quadrupole ($d$) and monopole ($s$) bosons which generate a U(6) algebra. Also, three limiting symmetries, U(5), O(6), and SU(3), have been considered which are dynamic symmetries for U(6). Moreover, for each of these symmetries, a specific group reduction chain provides the quantum numbers characterizing the states, which are suitable for a certain region of nuclei. Besides the advantage of unifying the group of theoretical descriptions of nuclei exhibiting different symmetries, the procedure defines very simple reference pictures for the limiting cases. For nuclei lying close to the region characterized by a certain symmetry, the perturbative corrections are to be included.

In Ref. [16], a new classification scheme was provided, all nuclei being distributed on the border of a symmetry triangle. The vertices of this triangle symbolize the U(5) (vibrator), O(6) ($\gamma$ soft), and SU(3) (symmetric rotor), while the legs of the triangle denote the transitional region. In Refs. [17,18], it was proved that on the U(5)-O(6) transition leg there exists a critical point for a second-order phase transition, while the U(5)-SU(3) leg has a first-order phase transition. In Ref. [19], it was proved that most nuclei are mapped not on the border of the symmetry triangle but in the interior of the triangle. Examples of such nuclei are the Os isotopes [20].

Recently, Iachello [21,22] pointed out that these critical points correspond to distinct symmetries, namely, E(5) and X(5). For the critical value of an ordering parameter, energies are given by the zeros of a Bessel function of half integer and irrational indices [23–25]. In Ref. [26], the X(5) description was extended to the first octupole vibrational band in nuclei close to axial symmetry and also close to the critical point of the U(5) to SU(3) phase transition. Other symmetries, called Y(5) and Z(5), were pointed out in Refs. [27,28]. The former symmetry corresponds to the critical point of the transition from axial to triaxial nuclei, while the latter one is related to the critical point of the transition from prolate to oblate through a triaxial shape.

The nice feature of the critical point symmetry is that the description in the intrinsic frame is performed by two separated differential equations for $\beta$ and $\gamma$ degrees of freedom. These equations are solvable, and the solutions are irreducible representations for the specific symmetry. Moreover, apart from an overall scaling parameter, the energies

 

are parameter-free quantities. Since the idea of symmetries associated with the critical points of various phase transitions appeared, many attempts have been made to describe the two dynamic deformations by solvable and separable differential equations with specific $\beta$ and $\gamma$ potentials. Thus, a description of soft $\gamma$ nuclei around $\gamma^0 = \frac{\pi}{6}$ with an oscillator potential in $\gamma$ and a Kratzer potential in $\beta$ has been developed in Refs. [29–31].

This paper is devoted also to the description of the triaxial nuclei. Indeed, the LDM Hamiltonian written in the intrinsic frame is separated into two terms describing the $\beta$ and $\gamma$ variables. The potential in $\beta$ consists of a centrifugal term and a sextic potential, while the differential equation for $\gamma$ is that for the Mathieu function. Due to this feature we shall call the formalism developed here as the sextic and Mathieu approach (SMA).

We state from the start that the equations for $\beta$ and $\gamma$ characterizing SMA are different from the $Z(5)$ formalism as well as from those using the Kratzer potential for $\beta$. The transition operator has an anharmonic structure. Theoretical features as well as the quantitative results are compared with those obtained within CSM. Moreover, a test for SMA is its application to several nonaxial nuclei like $^{188}$Os, $^{190}$Os, $^{192}$Os, $^{228}$Th, and $^{230}$Th.

The project presented above is achieved according the following plan. In Sec. II the derivation of the differential equations for $\beta$ and $\gamma$ is performed. In Sec. III, the needed equations for calculating the reduced transition probabilities are presented. The main ingredients of CSM are described in Sec. IV. In Sec. V we present the numerical application to five isotopes which are considered to have a triaxial shape. The final conclusions are drawn in Sec. VI.

## II. SEPARABLE FORM FOR THE LIQUID DROP MODEL HAMILTONIAN

The description of the triaxial nuclei proposed in the present paper originates from the eigenvalue equation:

$$H\psi(\beta,\gamma,\Omega) = E\psi(\beta,\gamma,\Omega), \tag{2.1}$$

where

$$H = -\frac{\hbar^2}{2B}\left[\frac{1}{\beta^4}\frac{\partial}{\partial\beta}\beta^4\frac{\partial}{\partial\beta} + \frac{1}{\beta^2\sin 3\gamma}\frac{\partial}{\partial\gamma}\sin 3\gamma\frac{\partial}{\partial\gamma} - \frac{1}{4\beta^2}\sum_{k=1}^{3}\frac{Q_k^2}{\sin^2\left(\gamma-\frac{2}{3}\pi k\right)}\right] + V(\beta,\gamma) \tag{2.2}$$

is the liquid drop model (LDM) Hamiltonian written in the intrinsic frame of reference. Here the dynamic deformation variables are denoted by $\beta$ and $\gamma$, the Euler angles by $\Omega \equiv (\theta_1,\theta_2,\theta_3)$, while the intrinsic angular momentum components by $Q_k$, with $k = 1, 2, 3$.

In what follows we shall describe a chain of approximations for Eq. (2.1) which allows us to treat separately the dynamic variables $\beta$ and $\gamma$, by exactly solvable differential equations.

The potential energy is chosen such that the differential equation (2.2) becomes separable. A possible form for $V(\beta,\gamma)$ is [32,33]

$$V(\beta,\gamma) = V_1(\beta) + \frac{V_2(\gamma)}{\beta^2}, \tag{2.3}$$

Inserting this expression into Eqs. (2.2) and (2.1) can be separated into two parts, one equation involving the $\beta$ variable and the other one the $\gamma$ variable and the Euler angles $\Omega$. Note that the equations of motion for the $\gamma$ variable and the Euler angles $\Omega$ are still coupled due to the rotational term

$$W = \frac{1}{4}\sum_{k=1}^{3}\frac{Q_k^2}{\sin^2\left(\gamma-\frac{2\pi}{3}k\right)}. \tag{2.4}$$

We separate the $\gamma$ variable from the Euler angles $\Omega$ in two steps. First we perform a second-order expansion of the $W$ term around $\gamma^0 = \pi/6$

$$W \sim \left(Q^2 - \frac{3}{4}Q_1^2\right) + 2\sqrt{3}\left(Q_2^2 - Q_3^2\right)\left(\gamma-\frac{\pi}{6}\right) + \left(10Q^2 - \frac{39}{4}Q_1^2\right)\left(\gamma-\frac{\pi}{6}\right)^2, \tag{2.5}$$

and then we average the result with the Wigner function $D^L_{MR}(\Omega)$

$$\langle W\rangle \sim L(L+1) - \frac{3}{4}R^2 + \left(10L(L+1) - \frac{39}{4}R^2\right)\times\left(\gamma-\frac{\pi}{6}\right)^2. \tag{2.6}$$

The Wigner function is the rotation operator matrix in the basis $|LM\rangle$ generated by the eigenstates of $Q^2$ and $Q_1$. Thus here the symmetry axis, obtained in the limit $\gamma \to \frac{\pi}{6}$, is the axis 1 and not 3 as it happens for situations characterized by $\gamma^0 = 0$. The term $L(L+1)$ from Eq. (2.6), multiplied by the factor $1/\beta^2$, is added to the $\beta$ equation:

$$\left[-\frac{1}{\beta^4}\frac{\partial}{\partial\beta}\beta^4\frac{\partial}{\partial\beta} + \frac{L(L+1)}{\beta^2} + v_1(\beta)\right]f(\beta) = \varepsilon_\beta f(\beta). \tag{2.7}$$

The remaining terms depend on $\gamma$ but also on $\beta$ by means of the factor $1/\beta^2$. In order that the variable separation is achieved, the mentioned factor is replaced by an average value $1/\langle\beta^2\rangle$. Actually in our concrete calculation, this is considered to be a free parameter. The resulting equation in $\gamma$ variable is

$$\left[-\frac{1}{\sin 3\gamma}\frac{\partial}{\partial\gamma}\sin 3\gamma\frac{\partial}{\partial\gamma} - \frac{3}{4}R^2 + \left(10L(L+1) - \frac{39}{4}R^2\right)\times\left(\gamma-\frac{\pi}{6}\right)^2 + v_2(\gamma)\right]\phi(\gamma) = \tilde{\varepsilon}_\gamma\phi(\gamma), \tag{2.8}$$

where the following notation is used:

$$v_1(\beta) = \frac{2B}{\hbar^2}V_1(\beta), \quad v_2(\gamma) = \frac{2B}{\hbar^2}V_2(\gamma), \quad \varepsilon_\beta = \frac{2B}{\hbar^2}E_\beta, \quad \tilde{\varepsilon}_\gamma = \langle\beta^2\rangle\frac{2B}{\hbar^2}E_\gamma. \tag{2.9}$$

To solve the separated equations in $\beta$ and $\gamma$, respectively, we have to specify the potentials $v_1(\beta)$ and $v_2(\gamma)$. Since $v_1(\beta)$ is

a sextic oscillator potential in $\beta$, we give a few details about the solution of the associated Schrödinger equation.

### A. Sextic oscillator with a centrifugal barrier

The Hamiltonian of the sextic oscillator with a centrifugal barrier has the expression [34,35]

$$H_x = -\frac{\partial^2}{\partial x^2} + \frac{\left(2s-\frac{1}{2}\right)\left(2s-\frac{3}{2}\right)}{x^2} + \left[b^2 - 4a\left(s+\frac{1}{2}+M\right)\right]x^2 + 2abx^4 + a^2x^6, \tag{2.10}$$

where $x \in [0,\infty)$. The classical counterpart of $H_x$ was studied in Ref. [36]. Analytical solutions for the classical trajectories have been found, which were then quantized. Also we note that for the particular value $a = 0$ the sextic potential becomes the Davidson potential [37]. Here we use the quantal form of the equation of motion and show that they yield also analytical solutions. To be concrete, the eigenvalue equation associated with Eq. (2.10) is quasi-exactly solvable for any values of $b$. Indeed, for any given non-negative integer $M$, it has $M+1$ solutions which can be found algebraically. This can be easily verified if we consider the Schrödinger equation

$$H_x\psi(x) = E\psi(x) \tag{2.11}$$

and take as an appropriate ansatz the function

$$\psi_n(x) = P_n(x^2)x^{2s-\frac{1}{2}}e^{-\frac{ax^4}{4}-\frac{bx^2}{2}}, \quad n = 0,1,2,\ldots, \tag{2.12}$$

where $P_n(x^2)$ is a polynomial in $x^2$ of degree $n$. Indeed, substituting Eq. (2.12) in Eq. (2.11) and eliminating the common factor, we obtain an equation for the $P_n(x^2)$:

$$QP_n(x^2) = EP_n(x^2), \tag{2.13}$$

with

$$Q = -\left(\frac{\partial^2}{\partial x^2} + \frac{4s-1}{x}\frac{\partial}{\partial x}\right) + 2b\left(x\frac{\partial}{\partial x} + 2s\right) + 2ax^2\left(x\frac{\partial}{\partial x} - 2M\right). \tag{2.14}$$

Now, let us assume that $M$ is a non-negative integer: $M = 0,1,2,\ldots$. In this case, the differential spectral equation (2.13) can easily be transformed into an algebraic form. The action of the $Q$ operator (2.14) on $P_n(x^2)$ gives again a polynomial in $x^2$ at the same order. Considering the coefficients of the polynomial $P_n(x^2)$ as components of an $(M+1)$ vector, one can treat Eq. (2.13) as an $(M+1)$-dimensional spectral matrix equation. This means that the initial Schrödinger equation (2.11) has at least $M+1$ solutions of the form (2.12) and thus can be interpreted as a quasi-exactly solvable equation of order $M+1$. For illustration, in the Appendix, we solve Eq. (2.13) for four particular values of $M$, i.e., $M = 0,1,2,3$.

The functions (2.12) can be normalized to unity for $a > 0$ and arbitrary $b$. Moreover for $a = 0$, the eigenvalue equation reduces to an ordinary oscillator equation. The norms of the wave functions can also be given in the closed form by using the result for the overlap integrals:

$$I^{(A)} = \int_0^\infty x^A e^{-\frac{a}{2}\beta^4 - b\beta^2}dx = \frac{1}{2}\Gamma\left(\frac{A+1}{2}\right)a^{-\frac{A+1}{4}} \times e^{\frac{b^2}{4a}}D_{-(A+1)/2}\left(\frac{b}{\sqrt{a}}\right), \tag{2.15}$$

$$= \frac{1}{2}\Gamma\left(\frac{A+1}{2}\right)(2a)^{(-A+1)/4}U\left(\frac{A+1}{4},\frac{1}{2},\frac{b^2}{2a}\right), \tag{2.16}$$

where $D_p(z)$ is the parabolic cylinder function and $U(\alpha,\delta;z)$ is one of the forms for the confluent hypergeometric function.

### B. Partial wave function depending on $\beta$

In Eq. (2.7), we make the change of function $f(\beta) = \beta^{-2}\varphi(\beta)$ and get

$$\left[-\frac{\partial^2}{\partial\beta^2} + \frac{L(L+1)+2}{\beta^2} + v_1(\beta)\right]\varphi(\beta) = \varepsilon_\beta\varphi(\beta). \tag{2.17}$$

We choose $v_1(\beta)$ such that Eq. (2.17) becomes the equation for a sextic oscillator potential with a centrifugal barrier. Indeed, this is achieved with the identifications

$$\begin{aligned} x &= \beta, \quad E = \varepsilon_\beta, \quad \left(2s-\frac{1}{2}\right)\left(2s-\frac{3}{2}\right) \\ &= L(L+1) \;\Rightarrow\; s = \frac{L}{2}+\frac{3}{4}, \\ v_1(\beta) &= (b^2-4ac)\beta^2 + 2ab\beta^4 + a^2\beta^6, \\ c &= \frac{L}{2}+\frac{5}{4}+M. \end{aligned} \tag{2.18}$$

This identification was possible after adding the term $-2/\beta^2$ to Eq. (2.7) and $2/\langle\beta^2\rangle$ to Eq. (2.8). In this way, the final centrifugal term in Eq. (2.17) will be $L(L+1)/\beta^2$. This trick ensures a rational form for $s$.

Suppose we fixed the constant parameters $a$ and $b$. Then, the potential depends on $c$ which at its turn depends on $L$ and $M$. It is desired that the potential be independent of angular momentum, that is, $c$ is a constant. Due to the equation relating $c$ and $L$

$$L = 2c - \tfrac{5}{2} - 2M, \tag{2.19}$$

this infers a certain dependence of $L$ on $M$. Indeed, to keep $c$ constant, it is necessary that increasing or decreasing $M$ by one unit should take place while decreasing or increasing $L$ by two units. So we get two constant values for $c$, one for $L$ even and other for $L$ odd:

$$(M,L): (k,0);(k-1,2);(k-2,4);(k-3,6)\cdots \Rightarrow c = k+\tfrac{5}{4} \equiv c^+ \;\; (L \text{ even}), \tag{2.20}$$

$$(M,L): (k,1);(k-1,3);(k-2,5);(k-3,7)\cdots \Rightarrow c = k+\tfrac{7}{4} \equiv c^- \;\; (L \text{ odd}). \tag{2.21}$$

The final form of the potential will be

$$v_1^\pi(\beta) = (b^2-4ac^\pi)\beta^2 + 2ab\beta^4 + a^2\beta^6 + u_0^\pi \quad (\pi \equiv \pm), \tag{2.22}$$

where $u_0^\pi$ are constants which will be fixed such that the minima ($\beta_{\min}^\pi > 0$) of the two potentials $v_1^+(\beta)$ and $v_1^-(\beta)$ have the same energy. The extremal points can be obtained from the first derivative of the potential:

$$\left.\frac{\partial v_1^\pi(\beta)}{\partial\beta}\right|_{\beta=\beta_0^\pi} = 0 \Rightarrow \left(\beta_0^\pi\right)^2 = 0,$$
$$\left(\beta_0^\pi\right)^2 = \frac{1}{3a}[-2b \pm \sqrt{b^2+12ac^\pi}]. \tag{2.23}$$

For $\beta_{\min} = 0$, we have $u_0^+ = u_0^-$. When $\beta_{\min} > 0$, we can set $u_0^+ = 0$, and from the condition $v_1^-(\beta_0^-) - v_1^+(\beta_0^+) = 0$, we get

$$u_0^- = (b^2-4ac^+)(\beta_0^+)^2 - (b^2-4ac^-)(\beta_0^-)^2 + 2ab[(\beta_0^+)^4 - (\beta_0^-)^4] + a^2[(\beta_0^+)^6 - (\beta_0^-)^6] \tag{2.24}$$

The shape of the potential $v_1^\pi(\beta)$ depends on the signs of $b^2-4ac^\pi$ and $b$. When $b > 2\sqrt{ac^\pi}$, the potential has a minimum at $\beta = 0$ and it increases monotonously with $\beta$. When $-2\sqrt{ac^\pi} < b < 2\sqrt{ac^\pi}$, a minimum shows up at $\beta > 0$, while for $b < -2\sqrt{ac^\pi}$, the potential has a maximum and a minimum.

The excitation energies for the $\beta$ equation are easily obtained using Eqs. (2.9) and (2.18).

$$E_\beta(n_\beta, L) = \frac{\hbar^2}{2B}\left[4bs(L) + \lambda_{n_\beta}^{(M)}(L) + u_0^\pi\right],$$
$$n_\beta = 0, 1, 2, \ldots, M. \tag{2.25}$$

As shown in the Appendix, the notation $\lambda_{n_\beta}^{(M)}$ is used for the eigenvalue corresponding to the eigenvector determining the coefficients defining the polynomial $P_n(x^2)$. Functions in the $\beta$ variable are given by Eq. (2.12) replacing $x$ with $\beta$

$$\varphi_{n_\beta,L}^{(M)}(\beta) = N_{n_\beta,L} P_{n_\beta,L}^{(M)}(\beta^2)\beta^{2s-\frac{1}{2}} e^{-\frac{a}{4}\beta^4 - \frac{b}{2}\beta^2},$$
$$n_\beta = 0, 1, 2, \ldots, M, \tag{2.26}$$

where $N_{n_\beta,L}$ are the normalization constants.

### C. Description of the $\gamma$ wave function

In what follows we show that Eq. (2.8) can be reduced to the Mathieu equation [38]. First we change the function

$$\phi(\gamma) = \frac{\mathcal{M}(3\gamma)}{\sqrt{|\sin 3\gamma|}}. \tag{2.27}$$

The equation for the new function is

$$\left[\frac{\partial^2}{\partial\gamma^2} + \left(\tilde{\varepsilon}_\gamma + \frac{1}{4} + \frac{3}{4}R^2\right) + \frac{9}{4\sin^2 3\gamma} - \left(10L(L+1) - \frac{39}{4}R^2\right)\left(\gamma - \frac{\pi}{6}\right)^2 - v_2(\gamma)\right]\mathcal{M}(3\gamma) = 0. \tag{2.28}$$

The potential in $\gamma$ is chosen to exhibit a minimum at $\gamma_0 = \pi/6$:

$$v_2(\gamma) = \mu\cos^2 3\gamma. \tag{2.29}$$

Making the Taylor expansions around the minimum value of the $\gamma$ potential

$$\frac{9}{4\sin^2 3\gamma} \sim \frac{9}{4} + \frac{81}{4}\left(\gamma - \frac{\pi}{6}\right)^2,$$
$$\mu\cos^2 3\gamma \sim 9\mu\left(\gamma - \frac{\pi}{6}\right)^2, \tag{2.30}$$

the equation for the variable $\gamma$ becomes

$$\left[\frac{\partial^2}{\partial\gamma^2} + \left(\tilde{\varepsilon}_\gamma + \frac{3}{4}R^2 + \frac{5}{2}\right) - \left(10L(L+1) - \frac{39}{4}R^2 + 9\mu - \frac{81}{4}\right)\left(\gamma - \frac{\pi}{6}\right)^2\right]\mathcal{M}(3\gamma) = 0. \tag{2.31}$$

Using again in Eq. (2.31) the approximation

$$\left(\gamma - \frac{\pi}{6}\right)^2 = \frac{1}{9}\cos^2 3\gamma, \tag{2.32}$$

and making the change of variable $y = 3\gamma$, we obtain

$$\left[\frac{\partial^2}{\partial y^2} + \frac{1}{9}\left(\tilde{\varepsilon}_\gamma + \frac{3}{4}R^2 + \frac{5}{2}\right) - \frac{1}{9}\left(\frac{10}{9}L(L+1) - \frac{13}{12}R^2 + \mu - \frac{9}{4}\right)\cos^2 y\right]\mathcal{M}(y) = 0. \tag{2.33}$$

This can be written in a compact form as

$$\left(\frac{\partial^2}{\partial y^2} + a - 2q\cos 2y\right)\mathcal{M}(y) = 0, \tag{2.34}$$

where

$$q = \frac{1}{36}\left(\frac{10}{9}L(L+1) - \frac{13}{12}R^2 + \mu - \frac{9}{4}\right),$$
$$a = \frac{1}{9}\left(\tilde{\varepsilon}_\gamma + \frac{3}{4}R^2 + \frac{5}{2}\right) - 2q. \tag{2.35}$$

Equation (2.34) is just the well-known Mathieu equation. Using the expression for the characteristic value $a$, Eq. (2.35), of the Mathieu equation, one can find the expression for the excitation energy of the $\gamma$ equation

$$E_\gamma(n_\gamma, L, R) = \frac{\hbar^2}{2B}\frac{1}{\langle\beta^2\rangle}\left[9a_{n_\gamma}(L, R) + 18q(L, R) - \frac{3}{4}R^2 - \frac{5}{2}\right], \quad n_\gamma = 0, 1, 2, \ldots. \tag{2.36}$$

The orthonormalization restriction for the Mathieu functions is

$$\int_0^{2\pi} \mathcal{M}_n(y)\mathcal{M}_m(y)dy = \pi\delta_{nm}. \tag{2.37}$$

The total energy for the system is obtained by adding the energies given by Eqs. (2.25) and (2.36)

$$E(n_\beta, n_\gamma, L, R) = E_0 + E_\beta(n_\beta, L) + E_\gamma(n_\gamma, L, R). \tag{2.38}$$

The excitation energies depend on four quantum numbers, $n_\beta$, $n_\gamma$, and $L$, $R$, and five parameters, $\hbar^2/2B$, $a$, $b$, $\frac{1}{\langle\beta^2\rangle}$, and $\mu$.

The quantum numbers defining the ground, $\beta$, and $\gamma$ bands are as follows:

$n_\beta = 0$, $n_\gamma = 0$, $R = L$, $L = 0, 2, 4, \ldots$ ground band,

$$n_\beta = 0, \quad n_\gamma = 1, \quad \begin{cases} R = L-2, L = 2,4,6,\ldots \\ R = L-1, L = 3,5,7,\ldots \end{cases} \gamma \text{ band},$$
$$n_\beta = 1, \; n_\gamma = 0, \quad R = L, \quad L = 0,2,4,\ldots \quad \beta \text{ band}. \tag{2.39}$$

.

## III. ELECTROMAGNETIC TRANSITIONS

The wave function describing the whole system is

$$|LRMn_\beta n_\gamma\rangle = N_{L,n_\beta} N_{L,R,n_\gamma} f_{L,n_\beta}(\beta)\phi_{L,R,n_\gamma}(\gamma) \times \sqrt{\frac{2L+1}{16\pi^2(1+\delta_{R0})}}\left[D^L_{MR}(\Omega) + (-1)^L D^L_{M-R}(\Omega)\right]. \tag{3.1}$$

The factors $N_{L,n_\beta}$ and $N_{L,R,n_\gamma}$ are related to the norms of the partial wave functions by

$$N^2_{L,n_\beta}\int_0^\infty \left|f_{L,n_\beta}(\beta)\right|^2\beta^4 d\beta = N^2_{L,n_\beta}\int_0^\infty \left|\varphi_{L,n_\beta}(\beta)\right|^2 d\beta = 1, \tag{3.2}$$

$$N^2_{L,R,n_\gamma}\int_0^{2\pi}\left|\phi_{L,R,n_\gamma}(\gamma)\right|^2|\sin 3\gamma|d\gamma = \frac{6}{\pi}\int_0^{\frac{\pi}{3}}\left|M_{L,R,n_\gamma}(3\gamma)\right|^2 d\gamma = 1. \tag{3.3}$$

Note that the integration over $\beta$ is performed with the measure $\beta^4 d\beta$, while that over $\gamma$ with the measure $|\sin 3\gamma|d\gamma$. These measures are characterizing the $(\beta,\ \gamma)$ space within the LDM. The wave functions just defined will be further used to calculate the reduced $E2$ transition probabilities.

In our approach, the quadrupole transition operator is defined as

$$T^{(E2)}_{2\mu} = t_1\alpha_{2\mu} + t_2[\alpha\times\alpha]_{2\mu}, \tag{3.4}$$

where $\alpha_{2\mu}$ denotes the quadrupole coordinates of the nuclear surface. The strengths $t_1$ and $t_2$ are free parameters which are fixed by fitting two particular $B(E2)$ values. The operator from Eq. (3.4) is written in the laboratory frame coordinates. Writing the quadrupole coordinates $\alpha_{2,\mu}$ in terms of intrinsic deformation variables $\beta$ and $\gamma$ and the Euler angles $\Omega$, one obtains for $T^{(E2)}_{2\mu}$, the following expression:

$$T^{(E2)}_{2\mu} = t_1\beta\left[\cos\left(\gamma-\frac{2\pi}{3}\right)D^2_{\mu 0} + \frac{1}{\sqrt{2}}\sin\left(\gamma-\frac{2\pi}{3}\right)\times\left(D^2_{\mu 2}+D^2_{\mu,-2}\right)\right] + t_2\sqrt{\frac{2}{7}}\beta^2\left[-\cos\left(2\gamma-\frac{4\pi}{3}\right)\times D^2_{\mu 0} + \frac{1}{\sqrt{2}}\sin\left(2\gamma-\frac{4\pi}{3}\right)\left(D^2_{\mu 2}+D^2_{\mu,-2}\right)\right]. \tag{3.5}$$

The argument $\gamma - 2\pi/3$ of the trigonometric functions is justified by the fact that it defines axis 1 of the principal inertial ellipsoid. Indeed, the transformation from the laboratory to the intrinsic frame is a rotation defined by the matrix $D^L_{MR}$, where the quantum numbers $M$ and $R$ are eigenvalues of the operator $Q_1$.

The reduced $E2$ transition probabilities are defined as

$$B(E2, J_i \to J_f) = \left|\langle J_i||T^{(E2)}_2||J_f\rangle\right|^2, \tag{3.6}$$

where Rose's convention [39] was used for the reduced matrix elements.

Summarizing the results obtained so far, we may say that the formalism proposed describes the $\beta$ variable by Eqs. (2.17) and (2.18), while $\gamma$ by Eq. (2.34). These equations provide for the total energy given by Eq. (2.38) a compact form. The wave functions obtained by solving the quoted equations, together with the transition operator of Eq. (3.5), are used to calculate the electric quadrupole transition probabilities. Conventionally we call the formalism proposed as the sextic and Mathieu approach (SMA).

Several groups have studied the $\gamma$ soft nuclei around $\gamma^0 = \frac{\pi}{6}$ [28–31]. Those approaches differ from the present formalism by the equations used for the description of $\beta$ and $\gamma$ coordinates.

Since the results of the SMA formalism will be compared with those obtained by the coherent state model (CSM), in what follows we shall briefly present its main ingredients.

## IV. COHERENT STATE MODEL (CSM)

The CSM defines [8] first a restricted collective space whose vectors are model states of ground, $\beta$, and $\gamma$ bands. In choosing these states we were guided by some experimental information which results in formulating a set of criteria to be fulfilled by the searched states.

All these required restrictions are fulfilled by the following set of three deformed quadrupole boson states:

$$\psi_g = e^{[d(b^\dagger_0 - b_0)]}|0\rangle \equiv T|0\rangle, \quad \psi_\gamma = \Omega^\dagger_{\gamma,2}\psi_g, \quad \psi_\beta = \Omega^\dagger_\beta\psi_g, \tag{4.1}$$

where the excitation operators for $\beta$ and $\gamma$ bands are defined by

$$\Omega^\dagger_{\gamma,2} = (b^\dagger b^\dagger)_{2,2} + d\sqrt{\frac{2}{7}}b^\dagger_{2,2},$$
$$\Omega^\dagger_\beta = (b^\dagger b^\dagger b^\dagger)_0 + \frac{3d}{\sqrt{14}}(b^\dagger b^\dagger)_0 - \frac{d^3}{\sqrt{70}}. \tag{4.2}$$

From the three deformed states, one generates through projection three sets of mutually orthogonal states

$$\varphi^i_{JM} = N^i_J P^J_{M0}\psi_i, \quad i = g,\beta,\gamma, \tag{4.3}$$

where $P^J_{MK}$ denotes the projection operator

$$P^J_{MK} = \frac{2J+1}{8\pi^2}\int D^{J^*}_{MK}\hat{R}(\Omega)\,d\Omega, \tag{4.4}$$

and $N^i_J$ are the normalization factors and $D^J_{MK}$ the rotation matrix elements. It was proved that the deformed and projected states contain the salient features of the major collective bands. Since we attempt to set up a very simple model, we rely on the experimental feature saying that the $\beta$ band is largely decoupled from the ground as well as from the $\gamma$ bands and choose a model Hamiltonian whose matrix elements between $\beta$ states and states belonging either to the

ground or to the $\gamma$ band are all equal to zero. The simplest Hamiltonian obeying this restriction is

$$H = A_1(22\hat{N} + 5\Omega^\dagger_{\beta'}\Omega_{\beta'}) + A_2\hat{J}^2 + A_3\Omega^\dagger_\beta\Omega_\beta, \quad (4.5)$$

where $\hat{N}$ is the boson number, $\hat{J}^2$ angular momentum squared, and $\Omega^\dagger_{\beta'}$ denotes

$$\Omega^\dagger_{\beta'} = (b^\dagger b^\dagger)_{00} - \frac{d^2}{\sqrt{5}}. \quad (4.6)$$

Higher-order terms in boson operators can be added to the Hamiltonian $H$ without altering the decoupling condition for the $\beta$ band. An example of this kind is the correction

$$\Delta H = A_4\left(\Omega^\dagger_\beta\Omega^2_{\beta'} + \text{H.c.}\right) + A_5\Omega^{\dagger 2}_{\beta'}\Omega^2_{\beta'}. \quad (4.7)$$

The energies for the $\beta$ band as well as for the $\gamma$ band states of odd angular momentum are described as average values of $H$ (4.5) or $H + \Delta H$ on $\varphi^\beta_{JM}$ and $\varphi^\gamma_{JM}$ ($J$ odd), respectively. As for the energies for the ground band and those of $\gamma$ band states with even angular momentum, they are obtained by diagonalizing a $2 \times 2$ matrix for each $J$.

The quadrupole transition operator is considered to be a sum of a linear term in bosons and one which is quadratic in the quadrupole bosons:

$$Q_{2\mu} = q_1(b^\dagger_{2\mu} + (-)^\mu b_{2,-\mu}) + q_2((b^\dagger b^\dagger)_{2\mu} + (bb)_{2\mu}). \quad (4.8)$$

The form of the anharmonic component of $Q_{2\mu}$ is justified by the fact that this is the lowest-order boson term that may connect the states from $\beta$ and ground bands in the vibrational limit, i.e., $d$ small.

Using the Rose convention, the reduced probability for the $E2$ transition $J^+_i \to J^+_f$ can be expressed as

$$B(E2; J^+_i \to J^+_f) = (\langle J^+_i||Q_2||J^+_f\rangle)^2. \quad (4.9)$$

Three specific features of CSM are worth mentioning:

(a) The model states are generated through projection from a coherent state and two excitations of that through simple polynomial boson operators. Thus, it is expected that the projected states may account for the semiclassical behavior of the nuclear system staying in a state of high spin.
(b) The states are infinite series of bosons, and thus highly deformed states can be described.
(c) The model Hamiltonian is not commuting with the boson number operator, and because of this property a basis generated from a coherent state is expected to be most suitable.

The CSM has been successfully applied to several nuclei exhibiting various equilibrium shapes which, according to the IBA (interacting boson approximation) classification, exhibit the SO(6), SU(5), and SU(3) symmetries, respectively. Several improvements of the CSM have been proposed by considering additional degrees of freedom such as isospin [9], quasiparticle [10], or collective octupole coordinates [11,12]. A review of the CSM achievements is found in Ref. [13].

## V. NUMERICAL RESULTS

The formalisms SMA and CSM presented in the previous sections have been applied for calculating the excitation energies and the available $B(E2)$ values for five isotopes: $^{188}$Os, $^{190}$Os, $^{192}$Os, $^{228}$Th, and $^{230}$Th. We start with the excitation energies analysis. As seen before, the total energy provided by SMA depends on five parameters: $\hbar^2/2B$, $a$, $b$, $\frac{1}{\langle\beta^2\rangle}$, and $\mu$. These were fixed by fitting the excitation energies using the least-squares procedure. The results are given in Table I. Concerning CSM, the parameters determining the energies are $d$, $A_1$, $A_2$, $A_3$. They were fixed as follows. We cycled $d$ within a large interval with a small step. For each $d$ we determined $A_1$ and $A_2$ by fitting the energies of two states, one belonging to the ground band and one from the $\gamma$ band. $A_3$ was obtained by fitting one level energy from the $\beta$ band. Then we chose that $d$ which yielded an overall good fit. The fitted parameters are given in Table I. Using the parameters from Table I, we can

TABLE I. Parameters $\hbar^2/2B$, $a$, $b$, $\frac{1}{\langle\beta^2\rangle}$, $\mu$ involved in the energy expression provided by SMA (2.38), are given for $^{188}$Os, $^{190}$Os, $^{192}$Os, $^{228}$Th, and $^{230}$Th. Also we give the values for the parameters $t_1$ and $t_2$ defining the transition operator used by SMA (3.5). The last six rows give the parameters determining the CSM excitation energies, $d$, $A_1$, $A_2$, $A_3$, and the specific $E2$ transition operators, i.e., $q_1$ and $q_2$.

| | $^{188}$Os | $^{190}$Os | $^{192}$Os | $^{228}$Th | $^{230}$Th |
|---|---|---|---|---|---|
| $\frac{\hbar^2}{2B}$ (keV) | 2.003 | 0.865 | 1.095 | 1.147 | 0.467 |
| $a$ | 932.16 | 4115.397 | 2497.596 | 1323.661 | 3041.51 |
| $b$ | 20 | 46.421 | 81 | −41.9 | 100 |
| $\frac{1}{\langle\beta^2\rangle}$ | 2.438 | 1.455 | 3.879 | 2.439 | 2.59 |
| $\mu$ | 296 | 3268 | 189 | 2936 | 9093 |
| $t_1$ | 5.608 ($e$ b) | 8.301 ($e$ b) | 7.591 ($e$ b) | $t_1$ | 136.0 [(W.u.)$^{1/2}$] |
| $t_2$ | 79.992 ($e$ b) | 426.959 ($e$ b) | 210.209 ($e$ b) | $3.376t_1$ | 1822.4 [(W.u.)$^{1/2}$] |
| $d$ | 2.35 | 2.05 | 1.5 | 3.14 | 3.16 |
| $A_1$ (keV) | 10.256 | 9.063 | 8.531 | 17.731 | 13.904 |
| $A_2$ (keV) | 14.336 | 15.679 | 14.490 | 15.122 | 2.650 |
| $A_3$ (keV) | 10.130 | 6.230 | 15.128 | −7.021 | −10.000 |
| $q_1$ | 0.132 ($10^{-1}$ $e$ b) | 0.105 ($10^{-1}$ $e$ b) | 0.437 ($10^{-1}$ $e$ b) | 15.927 ($e$ b) | 0.961 [(W.u.)$^{1/2}$] |
| $q_2$ | −0.226 ($e$ b) | −0.272 ($e$ b) | −0.315 ($e$ b) | −1.132 ($e$ b) | −1.255 [(W.u.)$^{1/2}$] |

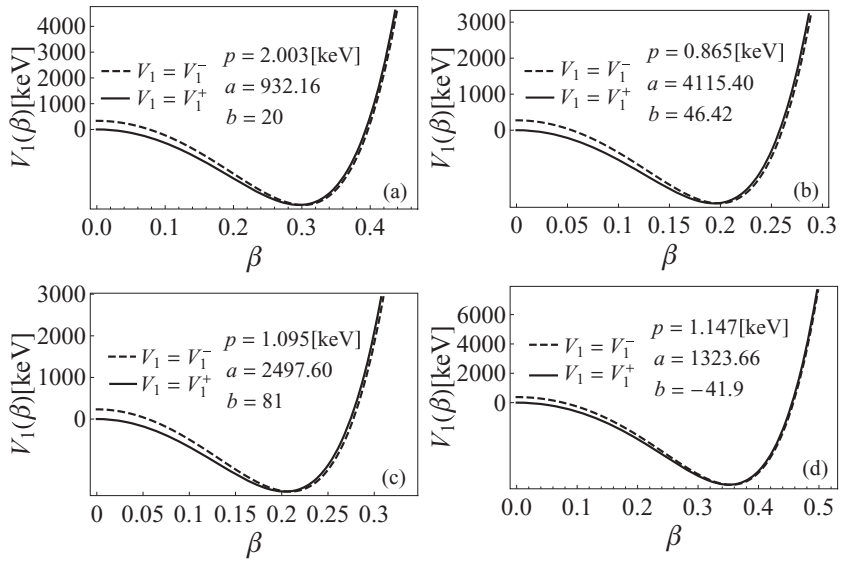


FIG. 1. Potentials $V_1^+(\beta)$ (full line) and $V_1^-(\beta)$ (dashed line) for $^{188}$Os (a), $^{190}$Os (b), $^{192}$Os (c), and $^{228}$Th (d). These potentials are given in keV.

draw the $\beta$ potentials characterizing SMA for the five nuclei. For a better representation, these plots are collected in Fig. 1 for the first four nuclei and in Fig. 5 for $^{230}$Th.

Note that the potentials have different minima points and different depths for the five isotopes considered in this paper. Also we notice that $V_1^-$ and $V_1^+$ are only slightly different, and that happens especially for small values of $\beta$. How the wave functions normalized to unity, for the potentials shown in Figs. 1 and 5 behave in a $\beta$ interval, is shown in Figs. 2 and 5, respectively. There are common features revealed by these pictures. Indeed, functions from ground and $\gamma$ bands have no node and one maximum located close to the potential minimum, while the function describing the state $0_\beta^+$ has one node and two extrema, the minimum being close to the potential minimum.

The $\gamma$ potential plots are given in Fig. 3 for each of the nuclei $^{188,190,192}$Os and $^{228}$Th. The potential for $^{230}$Th is given in Fig. 5.

Some plots of Mathieu functions corresponding to $^{188,190,192}$Os and $^{228}$Th are given in Fig. 4, while those for $^{230}$Th are in Fig. 5. Note that the functions for $0_g^+$ and $12_g^+$ are almost indistinguishable.

The excitation energies determined with the parameters listed in Table I are represented in Figs. 6–10. The results are compared with experimental data taken from Refs. [40–45]. The excitation spectra of the isotopes considered have been studied by different types of experiments. Thus Os isotopes were studied by Coulomb excitation using $^{40}$Ca, $^{58}$Ni, $^{138}$Xe, and $^{208}$Pb ions while $^{228}$Th by electron capture decay of $^{228}$Pa and alternatively by the reactions $^{230}$Th$(p, t)$ $^{228}$Th and $^{226}$Ra$(\alpha, 2n)^{228}$Th. As shown in Ref. [42], $^{230}$Th has been investigated by similar types of reactions. As seen in Figs. 6–10 all nuclei but $^{230}$Th have the common feature of having the $\beta$ band more excited than the $\gamma$ band. For this reason, we may say that all of them are $\gamma$ unstable nuclei.

There is a long-standing debate about the nature of the spectra characterizing Os isotopes. Some groups consider these nuclei as being $\gamma$ soft [4,46,47], while others as asymmetric rotor [5] which assumes rigidity in the $\gamma$ degrees of freedom. The equilibrium values, $\gamma^0$, predicted by Leander for

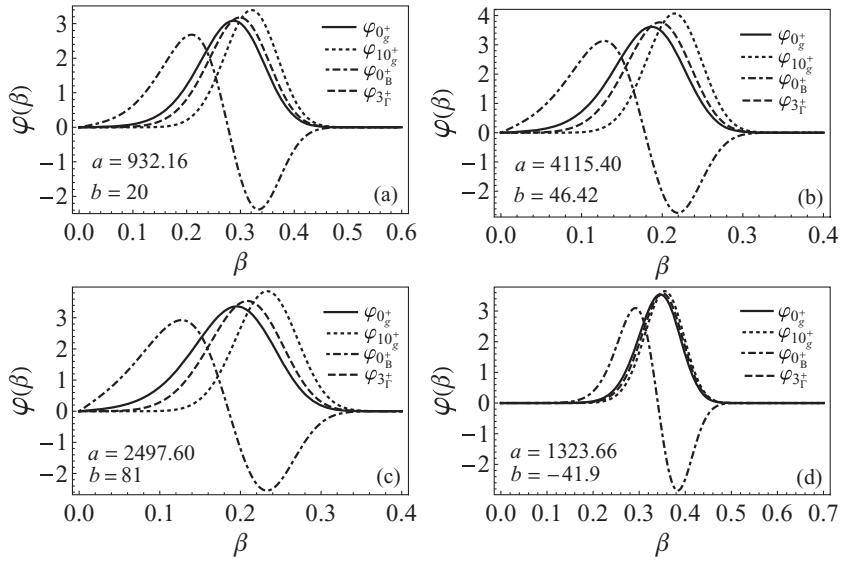


FIG. 2. Functions in $\beta$ variable for $^{188}$Os (a), $^{190}$Os (b), $^{192}$Os (c), and $^{228}$Th (d).

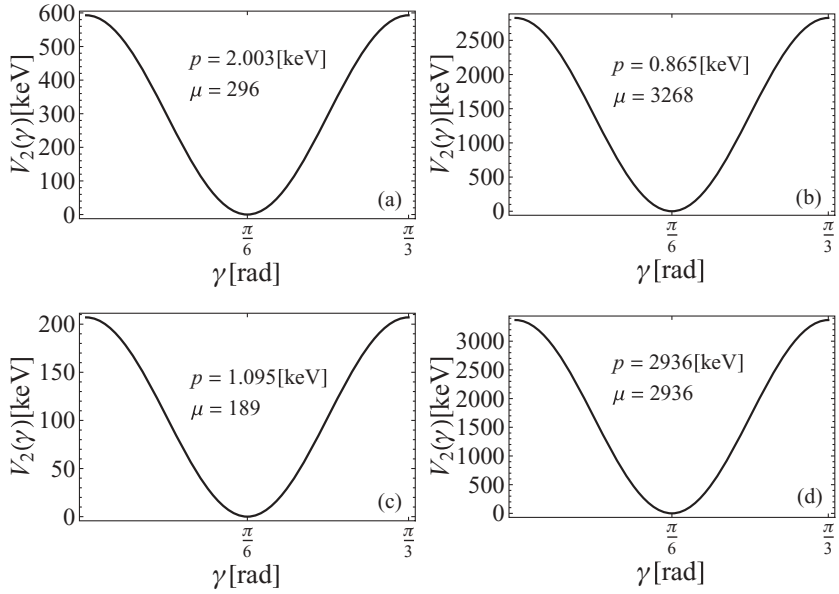


FIG. 3. Potentials $V_2(\gamma)$ for $^{188}$Os (a), $^{190}$Os (b), $^{192}$Os (c), and $^{228}$Th (d), given in keV.

$^{188,190,192}$Os in Ref. [47] are $20^0$, $20^0$, $25^0$, respectively, which might be considered closer to the $\gamma^0 = 30^0$ picture of the ideal triaxial liquid drop. The Os isotopes considered here have been treated [48] in terms of the IBA model in the transition region from the rotor to $\gamma$ unstable limit. Actually, in Ref. [49], these isotopes are considered textbook examples of this transition. The triaxial vibration rotation model (TRVM) [50] predicts for $^{228}$Th $\gamma^0 = 13^0$. One may ask why we add to the set of nuclei mentioned before the isotope $^{230}$Th. The reason is as follows. It is well known that the most distinctive signature of the triaxial rigid rotor is the equation relating the energies of three particular states

$$E_{2_1^+} + E_{2_2^+} = E_{3_1^+}. \tag{5.1}$$

Actually this equation is only approximately obeyed. Denoting by $\Delta E$ the modulus of the difference between the left- and right-hand sides of the mentioned relation, the experimental data for the five nuclei lead to the values

$$\Delta E = 2, 11, 5, 4, 8 \ \text{keV}, \tag{5.2}$$

for $^{188}$Os, $^{190}$Os, $^{192}$Os, $^{228}$Th, and $^{230}$Th, respectively. Clearly these deviations suggest that the nuclei considered in the present paper are close to an ideal triaxial rotor. As a matter of fact, this is the experimental feature which inspired us to take the $\gamma = 30^0$ as the reference picture. Deviations from this static situation were considered by a Taylor expansion. It is worth mentioning that the Th isotopes considered here have been found [51,52] to be located in the region with octupole vibration, as opposed to octupole deformation, the boarder between the two regions located at $^{224}$Th or $^{226}$Th [51–53]. One may say that the Th isotopes may be used to study not only the transition from $\gamma$ unstable to triaxial shapes but also the one from octupole deformed to octupole vibrational nuclei. It is an open question whether a quadrupole triaxial shape may favor the onset of the static octupole deformation.

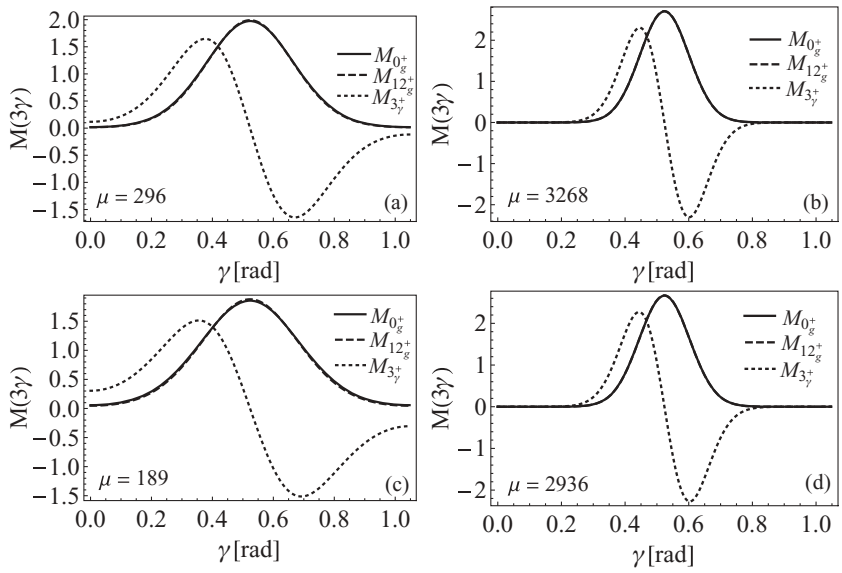


FIG. 4. Functions in $\gamma$ variable for $^{188}$Os (a), $^{190}$Os (b), $^{192}$Os (c), and $^{228}$Th (d).

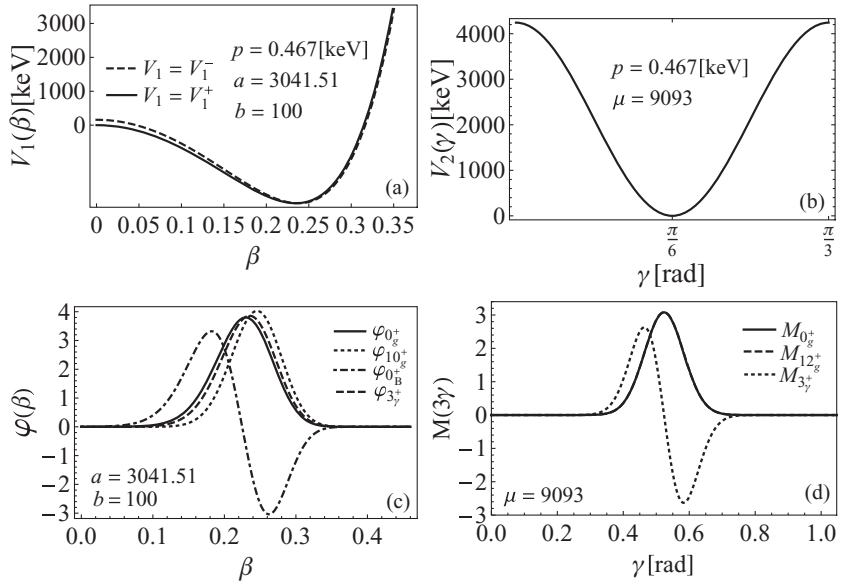


FIG. 5. Potentials for $\beta$ (a), $\gamma$ variables (b), some eigenfunctions in $\beta$ (c), and $\gamma$ (d) for $^{230}$Th.

The results of our calculations with SMA as well as with CSM are presented in Figs. 6–10. From these figures, we may conclude that the SMA procedure provides a reasonable quantitative description of the experimental data. Moreover, the two theoretical methods yield agreements with the data of similar quality.

Let us discuss now the results concerning the transition probabilities. The SMA made use of an anharmonic transition operator written in the intrinsic frame of reference (3.5), while CSM employs a second-order boson operator in the laboratory frame (4.8). In both cases the operators involve two parameters: $t_1$ and $t_2$ for SMA and $q_1$ and $q_2$ for CSM. These parameters were fixed by fitting two particular transitions for each nucleus. The fitted parameters are given in Table I. Experimental data for the five nuclei were taken from different sources, and for that reason they are presented in different manners.This is the reason for which the results for $^{228}$Th and $^{230}$Th are given in separate tables.

Inspecting Table II, we notice that both formalisms describe fairly well the intratransition in the ground and $\gamma$ bands. Concerning the transitions $J_\gamma^+ \to J_g^+$, we remark that they are quantitatively well described by both theoretical methods. CSM predicts for the $B(E2)$ associated with the transition $J_\gamma^+ \to (J-2)_g^+$ a value comparable to that corresponding to the transition $J_\gamma^+ \to J_g^+$. Concerning the transition $J_\gamma^+ \to (J+2)_g^+$, CSM predicts $B(E2)$ values small but comparable to the experimental data, while SMA yields vanishing values.

For $^{228}$Th we present, in Table III, results for some branching ratios which are compared with the corresponding

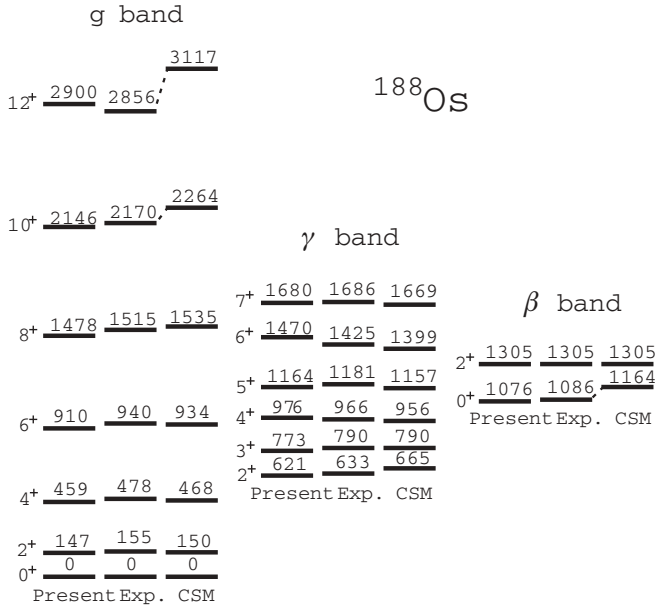


FIG. 6. Excitation energies, given in keV, for ground, $\beta$, and $\gamma$ bands of $^{188}$Os, calculated by the present approach (SMA) and CSM, compared with the corresponding experimental data [40,41].

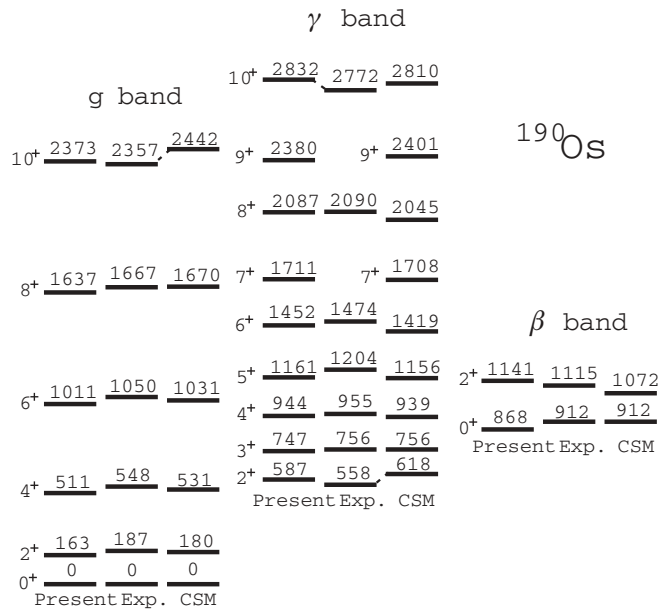


FIG. 7. Same as in Fig. 6, but for $^{190}$Os. Data are from Refs. [40,42].

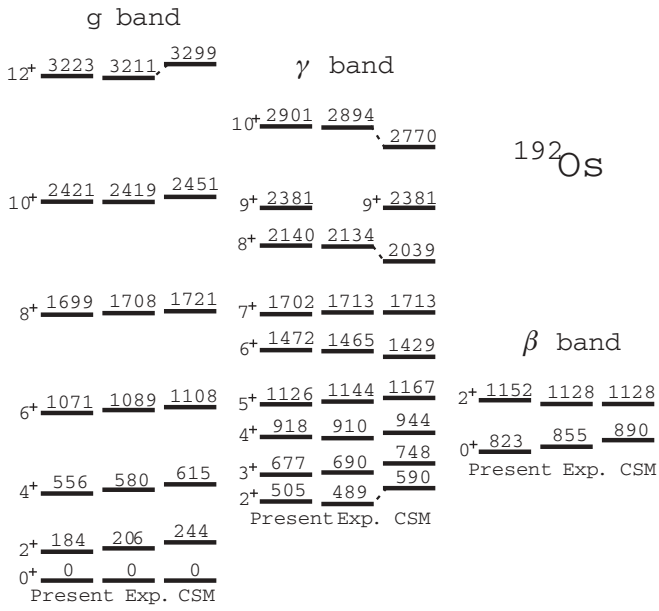


FIG. 8. Same as in Fig. 6, but for $^{192}$Os. Data are from Refs. [40,43].

data taken from Ref. [44]. Within SMA we determined the ratio $t_2/t_1$ by fitting one particular branching ratio. Thus, to determine $t_1$, information about a $E2$ transition is needed.

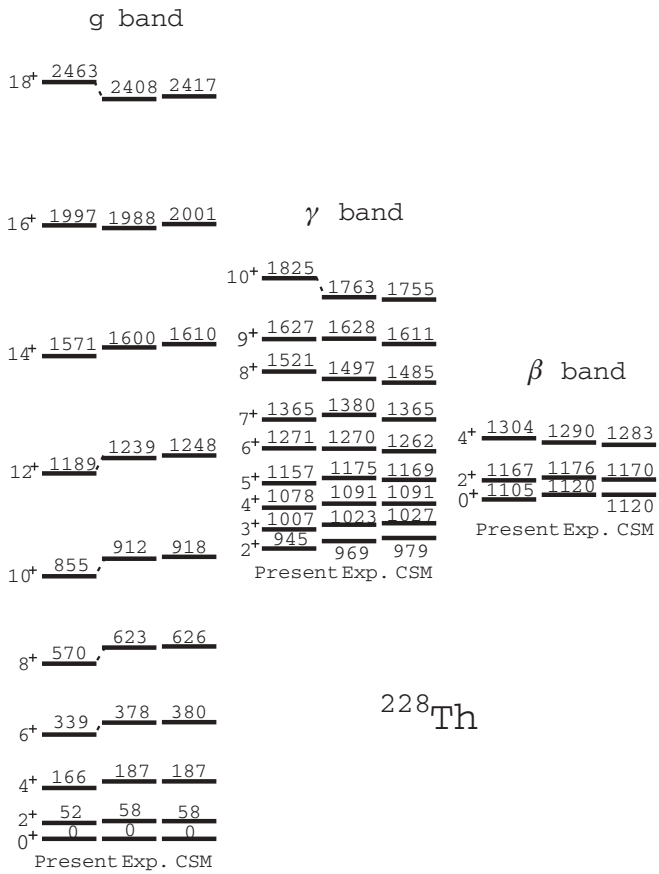


FIG. 9. Same as in Fig. 6, but for $^{228}$Th. Experimental data are from Ref. [44].

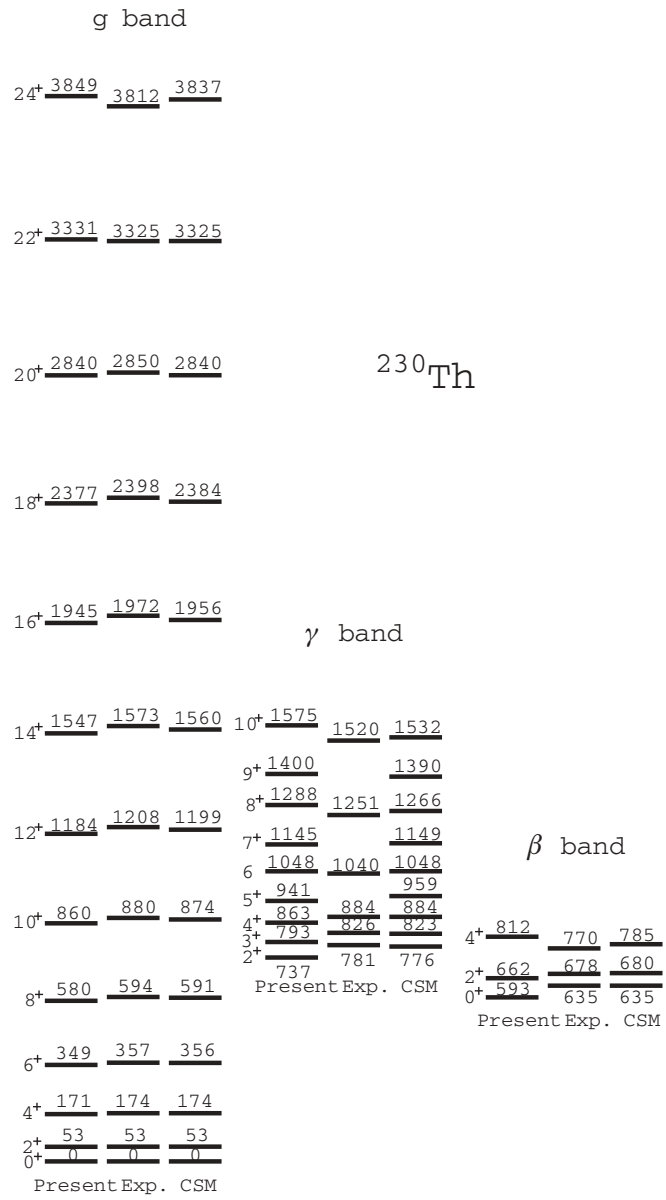


FIG. 10. Same as in Fig. 6, but for $^{230}$Th. Experimental data are from Ref. [45].

Theoretical results agree quite well with the data. Note again that the $B(E2)$ values of the transitions $2^+_\gamma \to 4^+_g$ and $4^+_\gamma \to 6^+_g$ provided by SMA are vanishing. The corresponding experimental data are small in magnitude.

The results for $^{230}$Th are listed in Table IV, where the experimental data taken from Ref. [45] are also given. We see that the intraband transitions have a collective character, while the interband ones are of the order of a Weisskopf unit, which is consistent with the commonly accepted definition of rotational bands.

As we mentioned before, a signature for triaxiality within the rigid rotor formalism is given by Eq. (5.1). Many authors investigated the transition from the $\gamma$ unstable regime to a triaxial behavior. The two nuclear phases are characterized by different doublet structures in the $\gamma$ band. While in the $\gamma$ unstable limit the $\gamma$-band levels form doublets arranged

TABLE II. Some $B(E2)$ values for $^{188,190,192}$Os obtained within two theoretical approaches, SMA and CSM, compared with the corresponding experimental data [40].

| $B(E2)$ $(e\,\mathrm{b})^2$ | $^{188}$Os | | | $^{190}$Os | | | $^{192}$Os | | |
|---|---|---|---|---|---|---|---|---|---|
| $J_i \to J_f$ | Expt. | SMA | CSM | Expt. | SMA | CSM | Expt. | SMA | CSM |
| $2_g^+ \to 0_g^+$ | 0.502 | 0.502 | 0.456 | 0.468 | 0.468 | 0.360 | 0.424 | 0.424 | 0.236 |
| $4_g^+ \to 2_g^+$ | 0.776 | 0.722 | 0.744 | 0.623 | 0.684 | 0.579 | 0.497 | 0.632 | 0.449 |
| $6_g^+ \to 4_g^+$ | 0.843 | 0.945 | 0.918 | 0.679 | 0.912 | 0.708 | 0.660 | 0.858 | 0.611 |
| $8_g^+ \to 6_g^+$ | 0.927 | 1.103 | 1.062 | 0.814 | 1.079 | 0.814 | 0.754 | 1.030 | 0.754 |
| $10_g^+ \to 8_g^+$ | 1.191 | 1.232 | 1.191 | 0.754 | 1.218 | 0.909 | 0.688 | 1.175 | 0.887 |
| $4_\gamma^+ \to 2_\gamma^+$ | 0.352 | 0.302 | 0.369 | 0.389 | 0.291 | 0.350 | 0.298 | 0.261 | 0.277 |
| $6_\gamma^+ \to 4_\gamma^+$ | 0.466 | 0.392 | 0.764 | 0.520 | 0.384 | 0.741 | 0.336 | 0.352 | 0.595 |
| $8_\gamma^+ \to 6_\gamma^+$ | 0.382 | 0.593 | 0.984 | 0.398 | 0.590 | 0.976 | 0.314 | 0.549 | 0.814 |
| $2_\gamma^+ \to 0_g^+$ | 0.047 | 0.005 | 0.165 | 0.039 | 0.001 | 0.202 | 0.037 | 0.006 | 0.192 |
| $2_\gamma^+ \to 2_g^+$ | 0.150 | 0.150 | 0.150 | 0.227 | 0.227 | 0.155 | 0.303 | 0.303 | 0.055 |
| $2_\gamma^+ \to 4_g^+$ | 0.029 | 0.000 | 0.001 | 0.007 | 0.000 | 0.001 | 0.024 | 0.000 | 0.000 |
| $4_\gamma^+ \to 2_g^+$ | 0.009 | 0.003 | 0.163 | 0.005 | 0.001 | 0.220 | 0.002 | 0.004 | 0.274 |
| $4_\gamma^+ \to 4_g^+$ | 0.134 | 0.031 | 0.202 | 0.229 | 0.050 | 0.229 | 0.203 | 0.068 | 0.137 |
| $4_\gamma^+ \to 6_g^+$ | 0.036 | 0.000 | 0.001 | 0.048 | 0.000 | 0.000 | 0.018 | 0.000 | 0.000 |
| $6_\gamma^+ \to 4_g^+$ | 0.001 | 0.002 | 0.194 | 0.003 | 0.001 | 0.269 | 0.000 | 0.002 | 0.357 |
| $6_\gamma^+ \to 6_g^+$ | 0.164 | 0.018 | 0.227 | 0.238 | 0.030 | 0.270 | 0.171 | 0.042 | 0.171 |

as $2^+, (3^+, 4^+), (5^+, 6^+), \ldots$, the rigid rotor doublets are $(2^+, 3^+), (4^+, 5^+), (6^+, 7^+), \ldots$. Transition from one regime to another has been studied by one of us (A.A.R.) in Ref. [12] within the CSM formalism. In the vibrational limit, the doublets of the $\gamma$ unstable picture become degenerate states. Going with deformation apart from zero, the degeneracy is lifted up, the doublet structure shows up, and for large deformation the doublet structure specific to triaxial shape is set on. The transition is also reflected in the dependence of the ratio

$$T_J = \frac{B(E2; (J+1)_\gamma^+ \to J_\gamma^+)}{B(E2; 2_g^+ \to 0_g^+)} \tag{5.3}$$

TABLE III. Some $B(E2)$ branching ratios for $^{228}$Th calculated alternatively within SMA and CSM, and compared with the corresponding experimental data [44].

| $B(E2)$ ratios | $^{228}$Th | | |
|---|---|---|---|
| $J_i; J_{f1}, J_{f2}$ | Expt. | SMA | CSM |
| $2_\gamma^+ \to 0_g^+$ | 0.450 | 0.450 | 0.450 |
| $\to 2_g^+$ | 1.000 | 1.000 | 1.000 |
| $\to 4_g^+$ | 0.031 | 0.000 | 0.064 |
| $3_\gamma^+ \to 2_g^+$ | 1.000 | 1.000 | 1.000 |
| $\to 4_g^+$ | 0.670 | 0.890 | 0.797 |
| $4_\gamma^+ \to 4_g^+$ | 1.000 | 1.000 | 1.000 |
| $\to 6_g^+$ | 0.062 | 0.000 | 0.017 |
| $2_\beta^+ \to 0_g^+$ | 0.410 | 0.374 | 0.590 |
| $\to 2_g^+$ | 1.000 | 1.000 | 1.000 |
| $\to 4_g^+$ | 4.200 | 1.800 | 1.870 |
| $4_\beta^+ \to 4_g^+$ | 1.000 | 1.000 | 1.000 |
| $\to 6_g^+$ | 4.700 | 1.247 | 1.490 |

on the deformation parameter $d$. In the limit of $d \to 0$, the function $T_J$ is vanishing for some angular momenta. In the first interval of $d$, $T_J$ is an increasing function then, it reaches a maximum value and then decreases. In the region of large $d$, the values $T_J$ are clustered in the same manner as the energy levels.

Another group [54,55] considers the level staggering in the $\gamma$ band as a sensitive signature for triaxiality. The doublet structure is reflected in the sawtooth shape of the function

$$S(J) = \frac{[E(J) - E(J-1)] - [E(J-1) - E(J-2)]}{E(2_g^+)}, \tag{5.4}$$

where $E(J)$ stands for the energy of the state $J^+$ belonging to the $\gamma$ band. It is worth noting that $S(J)$ is proportional to the discrete second derivative of $E(J)$ with respect to $J$. To see whether this signature is revealed also by the present approach, we plotted in Figs. 11 and 12 the function $S(J)$ for the nuclei considered here. As shown there, experimental evidence for staggering is found for $^{192}$Os, but very weak staggering can be

TABLE IV. Results for the $B(E2)$ values of a few transitions in $^{230}$Th, obtained within SMA and CSM formalisms, and compared with the corresponding experimental data [45].

| $B(E2)$ (W.u.) | $^{230}$Th | | |
|---|---|---|---|
| $J_i \to J_f$ | Expt. | SMA | CSM |
| $2_g^+ \to 0_g^+$ | 192 | 192 | 192 |
| $4_g^+ \to 2_g^+$ | 261 | 271 | 480 |
| $2_\beta^+ \to 0_g^+$ | 1.1 | 1.8 | 0.25 |
| $2_\beta^+ \to 4_g^+$ | 3.8 | 13.8 | 1.50 |
| $2_\gamma^+ \to 0_g^+$ | 3.0 | 0.34 | 5.49 |
| $2_\gamma^+ \to 2_g^+$ | 5.4 | 5.4 | 5.40 |
| $2_\gamma^+ \to 4_g^+$ | 0.35 | 0 | 0.10 |

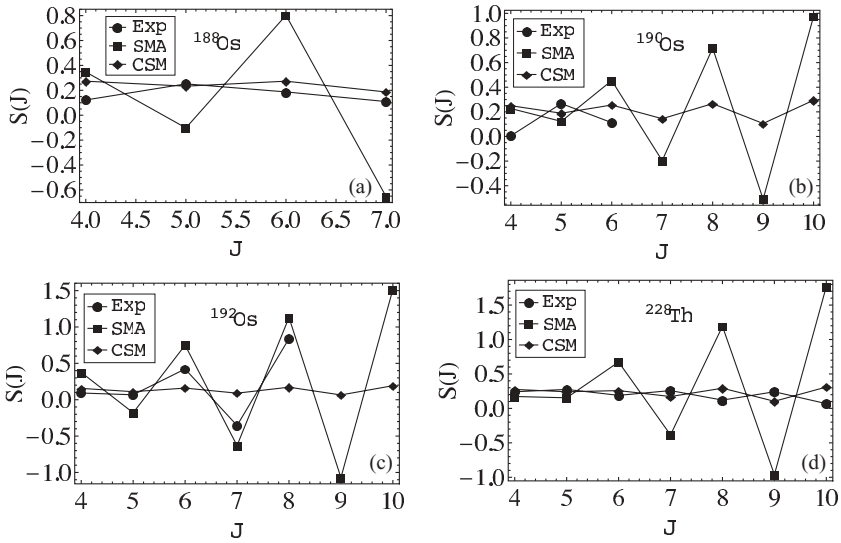


FIG. 11. Experimental and theoretical $S(J)$ for $^{188,190,192}$Os and $^{228}$Th.

seen in $^{188,190}$Os and $^{228}$Th. The staggering in $^{192}$Os is quite well described by SMA, while for the other mentioned nuclei, the CSM is closer to the experimental data. For $^{230}$Th, there are not enough relevant data, while the two formalisms, SMA and CSM, keep the pattern shown for other nuclei. We note that the oscillation amplitude of $S(J)$ is increasing with $J$. As mentioned before, the transition to a triaxial regime in CSM is determined by anharmonicities and quadrupole deformation. Within the SMA, which describes the deformations $\beta$ and $\gamma$ in the intrinsic frame, the triaxial shape is assumed from the beginning when a potential with a minimum in $\gamma_0 = \frac{\pi}{6}$ is chosen and the rotational term is expanded in powers of $\gamma$ around $\gamma = \frac{\pi}{6}$. Actually this is reflected in Fig. 11, which suggests an excess of staggering. It is interesting to notice that while Eq. (5.2) recommends $^{188,190}$Os and $^{228}$Th as exhibiting a triaxial shape, from Fig. 11 we see that experimental data as well as the CSM indicate that these nuclei show either no staggering ($^{188}$Os) or a weak staggering ($^{190}$Os and $^{228}$Th). In this context it is still unclear which of the two signatures, Eq. (5.1) or the level staggering in the $\gamma$ band, is more closely related to the shape triaxiality.

Triaxiality has been investigated within the IBA formalism in relation to various effects. Thus including higher-order terms, the triaxiality of $^{190,192}$Os has been studied in Ref. [56]. Including the $g$ boson, in a recent study [57] no shape or phase transition toward stable triaxial shapes was found. A phase diagram of IBA-2 (which distinguishes protons from neutrons) including triaxial shapes has been constructed in Refs. [58–60].

Triaxiality has recently been studied in the framework of the algebraic collective model [61], and the onset of rigid triaxial deformation has been considered [62].

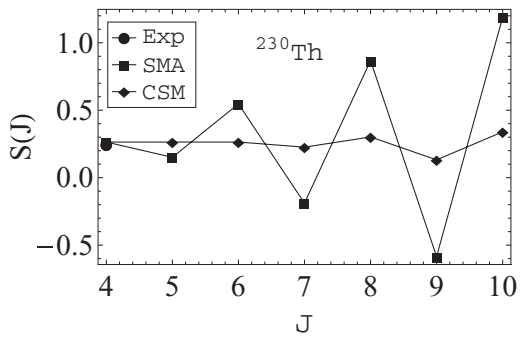


FIG. 12. Experimental and theoretical $S(J)$ for $^{230}$Th.

## VI. CONCLUSIONS

Here we summarize the main results obtained in the previous sections. The LDM Hamiltonian written in the intrinsic frame of reference was amended by a potential depending on the dynamic variables $\beta$ and $\gamma$ and chosen such that the equation for $\beta$ is separated from that for $\gamma$. The first equation is that for a sextic oscillator potential. Choosing as a trial function a product of a polynomial of degree $n$ and an exponential function, solving the differential equation is reduced to solving an simple eigenvalue equation of a known tridiagonal matrix having as eigenvectors the polynomial coefficients. In the limit of small deviation from the shape with $\gamma^0 = \frac{\pi}{6}$ the equation in $\gamma$ is obeyed by Mathieu functions. The formalism obtained is conventionally called the sextic and Mathieu approach (SMA). The total energy depends on five parameters which were fixed by a fitting procedure. Transition probabilities were treated by using an anharmonic transition operator involving two parameters which are to be determined by fitting two particular $B(E2)$ values.

The formalism was applied to five nuclei: $^{188,190,192}$Os, $^{228}$Th, and $^{230}$Th. The comparison with experimental data shows a good agreement between the corresponding results and data. We also compare the SMA results with those obtained with CSM. They are close to each other, although one is using intrinsic variables while the other is a boson description. Actually there is a strong reason for the closeness of the two quantitative descriptions. Indeed, following the procedure used in Ref. [63], one can show that the sextic oscillator equation can be derived starting with the CSM Hamiltonian, dequantizing it, treating the classical equations, and then quantizing them.

Also, by quantizing the classical variable $\gamma$ defined in the dequantized picture in the manner described in Ref. [64], one may obtain a Mathieu equation. Details about this comparison will be published elsewhere.

Before closing this section, we would like to mention that several authors have previously treated the $\gamma$ soft nuclei around $\gamma^0 = \frac{\pi}{6}$ [28–31]. However, their equations for $\beta$ as well for $\gamma$ variables are different from those proposed in the present paper. The $\beta$ potential is either an infinite square well [28] or a Coulomb or Kratzer potential [29–31]. Recently [65], the Davidson potential was used in relation to triaxial nuclei. Concerning $\gamma$, all quoted descriptions use an oscillator potential. The sextic potential was previously used in Ref. [34] but only for a few low-lying states. Again, the description of $\gamma$ is different.

As a final conclusion, SMA provides a realistic tool for the description of nuclei with equilibrium shapes close to $\gamma^0 = \frac{\pi}{6}$.

## ACKNOWLEDGMENT

This work was supported by the Romanian Ministry for Education Research Youth and Sport through the CNCSIS project ID-1038/2008.

## APPENDIX

Here we treat a few examples corresponding to $M = 0$, $M = 1$, $M = 2$, and $M = 3$.

The case $M = 0$:

$$P_n^{(0)}(x^2) = c_{00}, \quad 0c_{00} = \lambda c_{00},$$
$$E_n^{(0)} = 4bs + \lambda_n^{(0)} = 4bs, \quad \psi_n^{(0)}(x) \sim c_{00} x^{2s-\frac{1}{2}} e^{-\frac{ax^4}{4} - \frac{bx^2}{2}},$$
$$n = 0, 1, \ldots. \tag{A1}$$

Here we introduced the notation

$$\lambda \equiv E - 4bs. \tag{A2}$$

The case $M = 1$:

$$P_n^{(1)}(x^2) = c_{10} + c_{11}x^2,$$
$$\begin{pmatrix} 0 & -4(2s+0) \\ -4a & 4b \end{pmatrix} \begin{pmatrix} c_{10} \\ c_{11} \end{pmatrix} = \lambda \begin{pmatrix} c_{10} \\ c_{11} \end{pmatrix},$$
$$E_n^{(1)} = 4bs + \lambda_n^{(1)},$$
$$\psi_n^{(1)}(x^2) \sim \left[c_{10}\left(\lambda_n^{(1)}\right) + c_{11}\left(\lambda_n^{(1)}\right)x^2\right] x^{2s-\frac{1}{2}} e^{-\frac{ax^4}{4} - \frac{bx^2}{2}},$$
$$n = 0, 1, \ldots. \tag{A3}$$

The case $M = 2$:

$$P_n^{(2)}(x^2) = c_{20} + c_{21}x^2 + c_{22}x^4,$$
$$\begin{pmatrix} 0 & -4(2s+0) & 0 \\ -8a & 4b & -8(2s+1) \\ 0 & -4a & 8b \end{pmatrix} \begin{pmatrix} c_{20} \\ c_{21} \\ c_{22} \end{pmatrix} = \lambda \begin{pmatrix} c_{20} \\ c_{21} \\ c_{22} \end{pmatrix},$$
$$E_n^{(2)} = 4bs + \lambda_n^{(2)}, \quad \psi_n^{(2)}(x^2) \sim P_n^{(2)}(x^2) x^{2s-\frac{1}{2}} e^{-\frac{ax^4}{4} - \frac{bx^2}{2}},$$
$$n = 0, 1, \ldots. \tag{A4}$$

The case $M = 3$:

$$P_n^{(3)} = c_{30} + c_{31}x^2 + c_{32}x^4 + c_{33}x^6,$$
$$\begin{pmatrix} 0 & -4(2s+0) & 0 & 0 \\ -12a & 4b & -8(2s+1) & 0 \\ 0 & -8a & 8b & -12(2s+2) \\ 0 & 0 & -4a & 12b \end{pmatrix} \begin{pmatrix} c_{30} \\ c_{31} \\ c_{32} \\ c_{33} \end{pmatrix} = \lambda \begin{pmatrix} c_{30} \\ c_{31} \\ c_{32} \\ c_{33} \end{pmatrix},$$
$$E_n^{(3)} = 4bs + \lambda_n^{(3)}, \quad \psi_n^{(3)}(x^2) \sim P_n^{(3)}(x^2) x^{2s-\frac{1}{2}} e^{-\frac{ax^4}{4} - \frac{bx^2}{2}},$$
$$n = 0, 1, \ldots. \tag{A5}$$

Looking at the matrices obtained for the four cases considered above ($M = 0, 1, 2, 3$), it is clear that by induction one can write the matrix for a general case $M = k$, where $k \in N$. Actually this general form has been used to solve the sextic potential equation for high angular momenta. Details about solving the equation for a centrifugal plus sextic oscillator potential can be found in Ref. [66].

[1] A. Bohr, Mat. Fys. Medd. K. Dan. Vidensk. Selsk. **26**(14) (1952); A. Bohr and B. Mottelson, *ibid.* **27**(16) (1953).
[2] A. Faessler and W. Greiner, Z. Phys. **168**, 425 (1962); **170**, 105 (1962); **177**, 190 (1964); A. Faessler, W. Greiner, and R. Sheline, Nucl. Phys. **70**, 33 (1965).
[3] G. Gneus, U. Mosel, and W. Greiner, Phys. Lett. B **30**, 397 (1969).
[4] M. Seiwert, P. Hess, J. Maruhn, and W. Greiner, Phys. Rev. C **23**, 2335 (1981); P. Hess, J. Maruhn, and W. Greiner, J. Phys. G **7**, 737 (1981).
[5] A. S. Davydov and G. F. Filippov, Nucl. Phys. **8**, 237 (1958).
[6] A. S. Davydov and A. A. Chaban, Nucl. Phys. **20**, 499 (1960).
[7] A. S. Davydov, Nucl. Phys. **24**, 682 (1961).
[8] A. A. Raduta, V. Ceausescu, A. Gheorghe, and R. M. Dreizler, Phys. Lett. B **99**, 444 (1981); Nucl. Phys. A **381**, 253 (1982).
[9] A. A. Raduta, A. Faessler, and V. Ceausescu, Phys. Rev. C **36**, 2111 (1987).
[10] A. A. Raduta, C. Lima, and A. Faessler, Z. Phys. A **313**, 69 (1983).
[11] A. A. Raduta, Al. H. Raduta, and A. Faessler, Phys. Rev. C **55**, 1747 (1997); A. A. Raduta, D. Ionescu, and A. Faessler, *ibid.* **65**, 064322 (2002); A. A. Raduta, Al. H. Raduta, and C. M. Raduta, *ibid.* **74**, 044312 (2006).
[12] A. A. Raduta and C. Sabac, Ann. Phys. (NY) **148**, 1 (1983).
[13] A. A. Raduta, in *Recent Research Developments in Nuclear Physics*, Vol. 1, edited by S. G. Pandalai (Transworld Research Network, Karala, India, 2004), p. 1.

[14] A. Arima and F. Iachello, Ann. Phys. (N.Y.) **99**, 253 (1976); **123**, 468 (1979).
[15] F. Iachello and A. Arima, *The Interacting Boson Model* (Cambridge University, Cambridge, England, 1987).
[16] R. F. Casten, in *Interacting Bose-Fermi Systems in Nuclei*, edited by F. Iachello (Plenum, New York, 1981), p. 1.
[17] J. N. Ginocchio and M. W. Kirson, Phys. Rev. Lett. **44**, 1744 (1980) .
[18] A. E. L. Dieperink, O. Scholten, and F. Iachello, Phys. Rev. Lett. **44**, 1747 (1980).
[19] E. A. McCutchan, N. V. Zamfir, and R. F. Casten, Phys. Rev. C **69**, 064306 (2004).
[20] E. A. McCutchan and N. V. Zamfir, Phys. Rev. C **71**, 054306 (2005).
[21] F. Iachello, Phys. Rev. Lett. **85**, 3580 (2000).
[22] F. Iachello, Phys. Rev. Lett. **87**, 052502 (2001).
[23] R. F. Casten and N. V. Zamfir, Phys. Rev. Lett. **85**, 3584 (2000).
[24] R. F. Casten and N. V. Zamfir, Phys. Rev. Lett. **87**, 052503 (2001).
[25] P. G. Bizzeti and A. M. Bizzeti-Sona, Phys. Rev. C **66**, 031301 (R) (2002).
[26] P. G. Bizzeti and A. M. Bizzeti-Sona, Phys. Rev. C **81**, 034320 (2010).
[27] F. Iachello, Phys. Rev. Lett. **91**, 132502 (2003).
[28] D. Bonatsos, D. Lenis, D. Petrellis, and P. A. Terziev, Phys. Lett. B **588**, 172 (2004).
[29] L. Fortunato, Phys. Rev. C **70**, 011302 (2004).
[30] L. Fortunato, S. de Baerdemacker, and K. Heyde, Eur. Phys. J. A **25**, 439 (2005).
[31] L. Fortunato, S. de Baerdemacker, and K. Heyde, Phys. Rev. C **74**, 014310 (2006).
[32] L. Wilets and M. Jean, Phys. Rev. **102**, 788 (1956).
[33] L. Fortunato, Eur. J. Phys. **26**, s01 (2005).
[34] G. Lévai and J. M. Arias, Phys. Rev. C **69**, 014304 (2004).
[35] G. Lévai and J. M. Arias, Phys. Rev. C **81**, 044304 (2010).
[36] A. A. Raduta, F. D. Aaron, and I. I. Ursu, Nucl. Phys. A **772**, 20 (2006).
[37] P. M. Davidson, Proc. R. Soc. London Ser. A **135**, 459 (1932).
[38] A. A. Raduta, A. C. Gheorghe, P. Buganu, and A. Faessler, Nucl. Phys. A **819**, 46 (2009).
[39] M. E. Rose, *Elementary Theory of Angular Momentum* (Wiley, New York, 1957).
[40] C. Y. Wu *et al.*, Nucl. Phys. A **607**, 178 (1996).
[41] B. Singh, Nucl. Data Sheets **95**, 387 (2002).
[42] B. Singh, Nucl. Data Sheets **99**, 275 (2003).
[43] C. M. Baglin, Nucl. Data Sheets **84**, 717 (1998).
[44] J. Gröger *et al.*, Acta Phys. Pol. B **29**, 365 (1998).
[45] Y. A. Alcovali, Nucl. Data Sheets **69**, 155 (1993).
[46] K. Kumar and M. Baranger, Nucl. Phys. A **122**, 273 (1968).
[47] G. Leander, Nucl. Phys. A **273**, 286 (1976).
[48] R. F. Casten and J. A. Cizewski, Nucl. Phys. A **309**, 477 (1978).
[49] R. F. Casten, *Nuclear Structure from a Simple Perspective* (Oxford University, Oxford, 1990).
[50] U. Meyer, A. Faessler, and S. B. Khadkikar, Nucl. Phys. A **624**, 391 (1997); Prog. Part. Nucl. Phys. **38**, 241 (1997).
[51] D. Bonatsos, D. Lenis, N. Minkov, D. Petrellis, and P. Yotov, Phys. Rev. C **71**, 064309 (2005).
[52] D. Lenis and D. Bonatsos, Phys. Lett. B **633**, 474 (2006).
[53] P. G. Bizzeti and A. M. Bizzeti-Sona, Phys. Rev. C **77**, 024320 (2008).
[54] N. V. Zamfir and R. F. Casten, Phys. Lett. B **260**, 265 (1991).
[55] E. A. McCutchan, D. Bonatsos, N. V. Zamfir, and R. F. Casten, Phys. Rev. C **76**, 024306 (2007).
[56] G. Thiamova, Eur. Phys. J. **45**, 81 (2010).
[57] P. Van Isacker, A. Bouldjedri, and S. Serguine, Nucl. Phys. A **836**, 225 (2010).
[58] J. M. Arias, J. E. Garcia-Ramos, and J. Dukelsky, Phys. Rev. Lett. **93**, 212501 (2004).
[59] M. A. Caprio and F. Iachello, Ann. Phys. (NY) **318**, 454 (2005).
[60] M. A. Caprio and F. Iachello, Phys. Rev. Lett. **93**, 242502 (2004).
[61] D. J. Rowe, T. A. Welsh, and M. A. Caprio, Phys. Rev. C **79**, 054304 (2009).
[62] M. A. Caprio, Phys. Lett. B **672**, 396 (2009).
[63] A. A. Raduta, R. Budaca, and A. Faessler, J. Phys. G **37**, 085108 (2010).
[64] U. Meyer, A. A. Raduta, and A. Faessler, Nucl. Phys. A **637**, 321 (1998).
[65] I. Yigitoglu and D. Bonatsos, Phys. Rev. C **83**, 014303 (2011).
[66] A. G. Ushveritze, *Quasi-exactly Solvable Models in Quantum Mechanics* (IOP, Bristol, 1994).